Journal of Renewable Materials

Tech Science Press

DOI: 10.32604/jrm.2024.052579

ARTICLE

Conversion of Lignin into Porous Carbons for High-Performance Supercapacitors via Spray Drying and KOH Activation: Structure-Properties Relationship and Reaction Mechanism

Shihao Feng[1,2,3], Qin Ouyang[1,2,*], Jing Huang[1,2], Xilin Zhang[3], Zhongjun Ma[4], Kun Liang[1,2] and Qing Huang[1,2,*]

[1]Zhejiang Key Laboratory of Data-Driven High-Safety Energy Materials and Applications, Ningbo Key Laboratory of Special Energy Materials and Chemistry, Ningbo Institute of Materials Technology and Engineering, Chinese Academy of Sciences, Ningbo, 315201, China

[2]Engineering Laboratory of Advanced Energy Materials, Qianwan Institute of CNITECH, Ningbo, 315336, China

[3]School of Physics, Henan Normal University, Xinxiang, 453007, China

[4]School of Environment, Henan Normal University, Xinxiang, 453007, China

[*]Corresponding Authors: Qin Ouyang. Email: ouyangqin@nimte.ac.cn, o_yang@126.com; Qing Huang. Email: huangqing@nimte.ac.cn

Received: 07 April 2024 Accepted: 27 May 2024 Published: 21 August 2024

ABSTRACT

Lignin-derived porous carbons have emerged as promising electrode materials for supercapacitors. However, the challenge remains in designing and controlling their structure to achieve ideal electrochemical performance due to the complex molecular structure of lignin and its intricate chemical reactions during the activation process. In this study, three porous carbons were synthesized from lignin by spray drying and chemical activation with varying KOH ratios. The specific surface area and structural order of the prepared porous carbon continued to increase with the increase of the KOH ratio. Thermogravimetric-mass spectrometry (TG-MS) was employed to track the molecular fragments generated during the pyrolysis of KOH-activated lignin, and the mechanism of the thermochemical conversion was investigated. During the thermochemical conversion of lignin, KOH facilitated the removal of H_2 and CO, leading to the formation of not only more micropores and mesopores, but also more ordered carbon structures. The pore structure exhibited a greater impact than the carbon structure on the electrochemical performance of porous carbon. The optimized porous carbon exhibited a capacitance of 256 F g^{-1} at a current density of 0.2 A g^{-1}, making it an ideal electrode material for high-performance supercapacitors.

KEYWORDS

Lignin; porous carbon; KOH activation; mechanism; supercapacitor

1 Introduction

Lignocellulose is the most plentiful renewable resource globally, accounting for about 50% of carbon resources and is considered a viable substitute for fossil fuels [1]. Lignocellulose-derived carbon materials are widely used in green energy storage devices, and their properties depend on the composition and structure of lignin, cellulose, and hemicellulose [2–4]. Lignin contributes the most to the lignocellulose-

derived carbon materials due to its high carbon content and high carbonization yield [5,6]. Industrial lignin, which exceeds 70 million tons per year as a major by-product of pulp and paper and biofuel production, is readily available but underutilized [7,8]. Developing an efficient method to prepare lignin-based functional materials with well-regulated morphology, structure, and excellent properties is crucial for realizing high-value utilization of lignin [9–13].

Recently, porous carbons derived from lignin have become promising electrode materials for supercapacitors [14,15]. The preparation of porous carbons involves a crucial activation process, which significantly influences the pore structure and electrochemical performance [16–20]. Chemical activators such as KOH, K_2CO_3 and $ZnCl_2$ are often used to prepare porous carbon [21,22]. Among these activators, KOH is the most widely used one since it can produce porous carbon with a high micropore volume, a narrow pore size distribution, and a very high specific surface area of up to 3000 $m^2\ g^{-1}$ [23]. The pore structure and elemental composition of KOH-activated porous carbon seriously depend on the activation parameters (ratio of sample to KOH, time and activation temperature, etc.) and the carbon source used. Many researchers have used lignin as a raw material and KOH as an activator to prepare porous carbons. Wang et al. successfully synthesized lignin-based carbon aerogel using lignin sulfate as the raw material and KOH as the activator. The obtained carbon aerogels exhibited a remarkable specific surface area of 3742 $m^2\ g^{-1}$ and an impressive porosity of 1.881 $cm^3\ g^{-1}$ [24]. Wang et al. prepared porous carbon materials with a specific surface area of 3130 $m^2\ g^{-1}$ by employing urea-modified lignin as the raw material and KOH as the activator [25]. These lignin-derived porous carbons synthesized by KOH activation exhibit high specific surface area and micropore volume, showing significant advantages in energy storage applications.

Although KOH activation is a well-known method for forming porous carbon networks, the activation mechanism is still not well understood due to the complexity of the chemical reactions. Otowa et al. reported the activation process of petroleum coke by KOH at a temperature below 700°C and found that the reaction products during the KOH activation process were mainly H_2, CO, CO_2, K_2O and K_2CO_3 [26]. When lignin is used as a carbon source and activated by KOH, its complex and diverse composition makes the activation process more complex. To our knowledge, there are few related studies on the mechanism of KOH activation of lignin. As an abundant natural carbon source, lignin is a promising precursor for porous carbons, it is necessary to understand the structural transformation mechanism of lignin during KOH activation, which will help us to precisely synthesize lignin-derived porous carbon with desired structure and properties.

In this work, lignin-derived porous carbons were prepared by a scalable spray-drying technique followed by KOH activation. In order to study the mechanism of KOH activation of lignin, Thermogravimetry-mass spectrometry (TG-MS) was employed to monitor the molecular fragments generated during the pyrolysis of KOH-activated lignin. The effect of KOH on the chemical conversion of lignin to porous carbons was analyzed. The structure of lignin-derived porous carbons was characterized by XRD, Raman and TEM. The electrochemical properties of the lignin-derived porous carbons were investigated for their potential application in electrical double-layer capacitors (EDLCs) using cyclic voltammetry, galvanostatic charge-discharge techniques, and electrochemical impedance spectroscopy.

2 Experimental

2.1 Materials

A commercial sodium lignosulfonate (SLS) was provided by Shanghai Aladdin (Shanghai, China) and used as the raw material of porous carbons. Polyvinylpyrrolidone (PVP) was obtained from the same supplier and employed as a binder for particle forming. KOH and HCl were provided by Sinopharm Chemical Reagent (Shanghai, China). All the materials were used directly without any additional treatment.

2.2 Preparation

A 20% aqueous solution of SLS was prepared, followed by the addition and dissolution of 1% PVP relative to SLS. Subsequently, lignin powders were obtained from the SLS solution using a centrifugal spray dryer with an inlet temperature of 150°C.

The lignin powders were converted into porous carbons through a simple curing and KOH activation method [27]. The lignin powders underwent curing at 300°C for 1 h, followed by immersion in KOH solution with three different sample-to-KOH ratios (1:1, 1:2, and 1:3). The KOH-treated powders were then dried and carbonized at 800°C for 2 h. They were then washed with a 1M HCl solution and deionized water multiple times. After drying at 80°C for 12 h, three distinct porous carbon samples were obtained and labeled as PC-1, PC-2 and PC-3, respectively.

2.3 Characterization

A JSM 7500F scanning electron microscope was employed to characterize the lignin powders and porous carbons. The pyrolysis process of the KOH-modified powders was studied using a Netzsch STA 449F3 thermal analyzer-mass spectrometry system under an Ar atmosphere with a heating rate of 10°C/min. The porous carbons were characterized through X-ray diffraction (ADVANCE D8, Saarbrucken, Germany), Raman spectroscopy (LAbRAMHR Evolution, Paris, France), high-resolution transmission electron microscopy (JEM-2100, Akishima-shi, Tokyo, Japan), and nitrogen adsorption analyses (ASAP 2460, Micromeritics, Atlanta, GA, USA). The electrochemical characteristics of the porous carbons used as electrode materials in supercapacitors were evaluated using the same method as reported in our previous work [27].

3 Results and Discussion

3.1 Morphology and Structure of Porous Carbons

Fig. 1 shows the SEM images of the lignin powder and porous carbons. As shown in Fig. 1a, the lignin powder exhibits a unique shrunken dimple shape. It is related to the inlet temperature during the spray drying process [27]. Porous carbons with varying morphologies have been prepared from the same lignin powder by adjusting the ratio of the sample to KOH. Specifically, when the ratio of sample to KOH is 1:1, the obtained porous carbon keeps the shrunken dimple shape of the lignin powder, but forms a porous structure on the surface (Fig. 1b). Upon increasing the ratio to 1:2, the original particle morphology is completely altered, transforming into a foam skeleton structure (Fig. 1c). Increasing the ratio to 1:3 results in the sample transformation from a foam structure to nanosheets (Fig. 1d). The sudden shift in the morphology of porous carbons is primarily due to the etching effect of KOH. KOH reacts with the carbon of lignin molecules, resulting in the original three-dimensional amorphous structure of lignin being destroyed and transformed into a layered carbon structure.

The pore structure of the porous carbons was analyzed through nitrogen adsorption and desorption isotherm measurements, and the results are presented in Fig. 2 and Table 1. As shown in Fig. 2a, the porous carbon samples, namely PC-1, PC-2 and PC-3, display a blend of type I and type IV isotherms. At extremely low relative pressure ($P/P_0 < 0.01$), the adsorbed amount rises sharply, and a hysteresis loop is observed between P/P0 = 0.45 and 0.9. The hysteresis loop is attributed to the capillary condensation of nitrogen molecules in mesoporous pores. The characteristics of these isotherms indicate that all the samples have micropores and mesopores. As shown in Fig. 2b, the pore size distribution of the three samples is primarily composed of micropores and mesopores. With the increase of the KOH ratio, the specific surface area gradually increases. The specific surface area of PC-1 is 1417 $m^2\ g^{-1}$, while PC-2 has a value of 2060 $m^2\ g^{-1}$ and PC-3 reaches 2475 $m^2\ g^{-1}$. The total pore volume is also increasing, with values of 0.77 $cm^3\ g^{-1}$ for PC-1, 1.11 $cm^3\ g^{-1}$ for PC-2, and 1.33 $cm^3\ g^{-1}$ for PC-3. PC-1 is dominated by micropores (V_{micro} = 0.62 cm^3/g), with a small number of mesopores (V_{Meso} = 0.02 cm^3/g). The increase in KOH ratio leads to an increase in the volume of mesopores, while

simultaneously reducing the volume of micropores. PC-3 is dominated by mesopores (V_{Meso} = 1.11 cm^3/g), with a drastic reduction in its micropore volume (V_{micro} = 0.12 cm^3/g). Generally speaking, KOH activation includes radial activation and lateral activation. The former will lead to the formation of micropores, while the latter will expand the space of micropores and form mesopores.

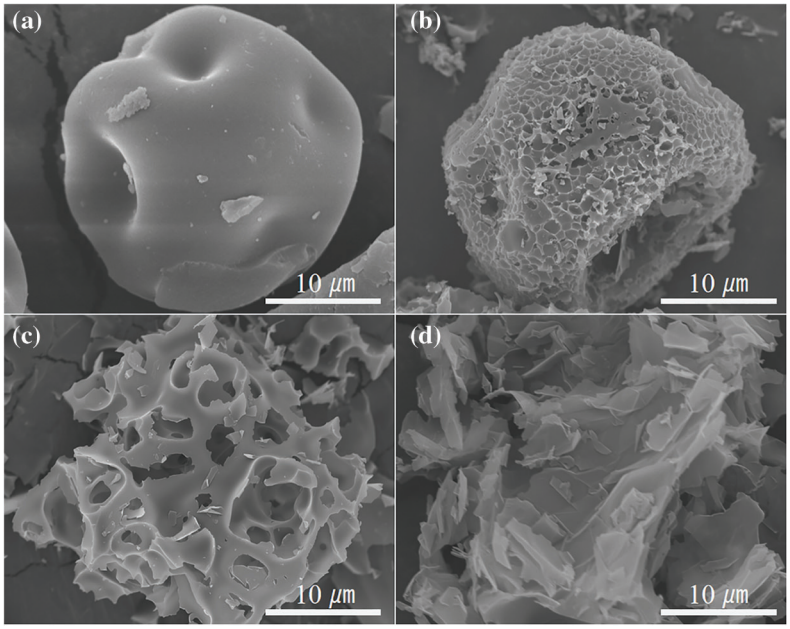

Figure 1: SEM images of (a) lignin powders, (b) PC-1, (c) PC-2 and (d) PC-3

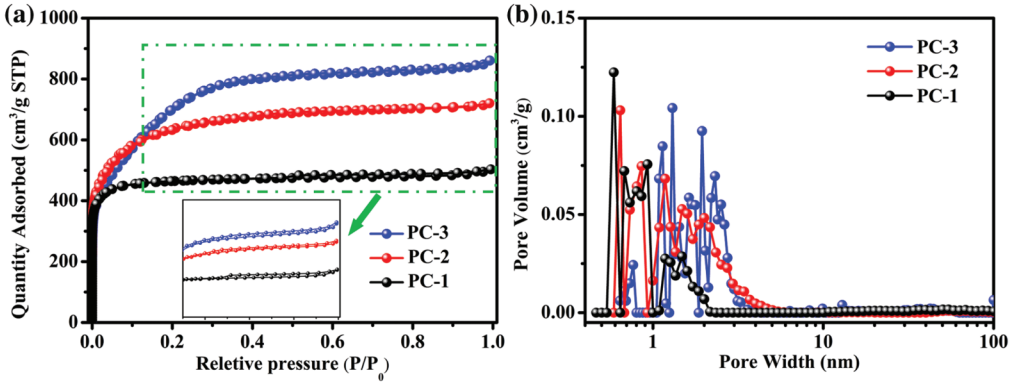

Figure 2: (a) Nitrogen adsorption/desorption isotherms and (b) BJH pore size distributions of PC-1, PC-2, and PC-3 were generated through activation with varying ratios of sample to KOH

Table 1: Pore properties of the lignin-derided porous carbons

Sample	SSA (m^2/g)	TPV (cm^3/g)	V_{micro} (cm^3/g) < 0.7 nm	< 2 nm	V_{Meso} (cm^3/g)	PSD (nm)
PC-1	1417	0.77	0.19	0.62	0.02	2.7
PC-2	2060	1.11	0.15	0.57	0.34	2.4
PC-3	2475	1.33	0.10	0.12	1.11	2.2

Note: SSA: specific surface area. TPV: total pore volume. V_{micro}: micropore volume. V_{Meso}: mesopore volume. PSD: pore size distribution calculated by the formula PSD = 4TPV/SSA.

In Fig. 3a, the XRD patterns of the porous carbons activated with varying KOH ratios are presented. Both PC-1 and PC-2 exhibit a minor peak at 26.6°, suggesting the existence of a limited amount of ordered structure within the porous carbons. Upon increasing the ratio of sample to KOH to 1:3, the XRD pattern of the resulting PC-3 sample displays a distinct peak at 26.6°, indicating a highly ordered and crystalline structure. The results show that a higher concentration of KOH can promote the formation of more ordered carbon. In Fig. 3b, the Raman spectra of the porous carbons are illustrated. Two significant peaks at approximately 1351 and 1585 cm^{-1}, identified as D band and G band, respectively, are evident. The D band is associated with the defect and disorder of the carbon, while the G band corresponds to the in-plane bond stretching pattern of the C-C bond in the graphite structure. The D and G bands of PC-1 and PC-2 are broad and overlapping, indicating that they are predominantly amorphous. In comparison, PC-3 exhibits a weak D band, a sharp and strong G band and a distinct peak at around 2714 cm^{-1}, which corresponds to the 2D band. These features suggest that PC-3 has a graphite-like structure. The intensity ratio of the D band to the G band (I_D/I_G) is commonly employed to assess the level of order of carbon materials. A lower I_D/I_G ratio signifies a higher degree of order in the carbon materials. The I_D/I_G ratios of PC-1, PC-2 and PC-3 are 1.25, 1.19 and 0.21, respectively. The I_D/I_G value of PC-3 is the lowest, indicating the highest degree of order, which is consistent with the XRD results. Fig. 4 shows the TEM/HRTEM images and SAED pattern of PC-3. The layer structure of graphite can be clearly observed in the HRTEM image. It indicates that PC-3 indeed has a high degree of structural order. The appearance of graphite-like structure in PC-3 has further confirmed that KOH activation contributes to the improvement of the structural order of lignin-derived porous carbon. There are similar reports in the literature [28], but the mechanism that how KOH converts amorphous carbon into ordered carbon at a low temperature is still unclear.

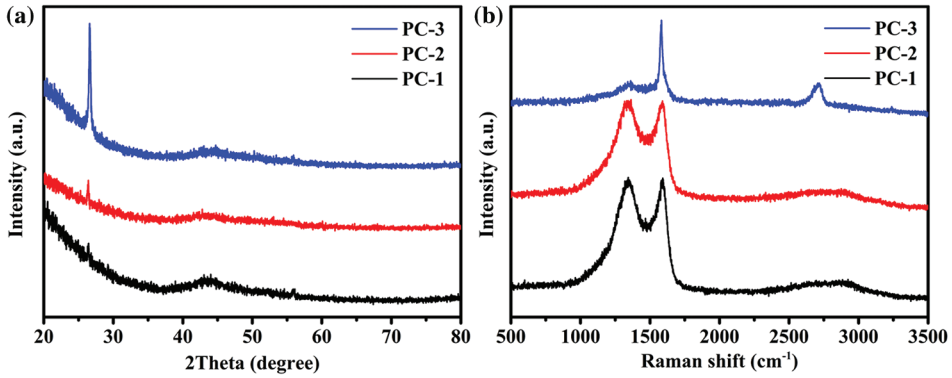

Figure 3: (a) XRD patterns and (b) Raman spectra of the porous carbons

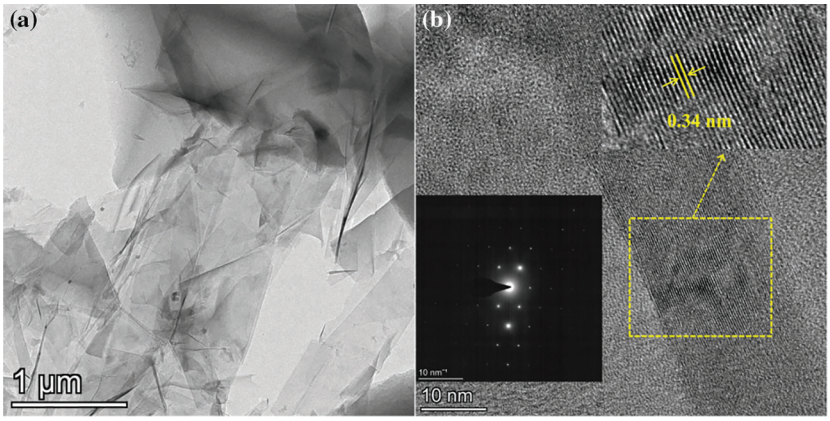

Figure 4: (a) TEM/HRTEM images and (b) SAED pattern of PC-3

3.2 Reaction Mechanism of KOH Activation

Fig. 5 shows the TG/DTG curves of the cured lignin powder LP-300 and the KOH-modified LP-300 for the preparation of PC-3. LP-300 exhibits a slight weight loss below 200°C, because it has been previously cured at 300°C. LP-300 mainly undergoes two severe weight-loss stages, showing two peaks at about 413°C and 708°C in the DTG curve. A residual mass of about 60% is obtained at 800°C, which indicates that lignin has a relatively high carbonization yield. KOH-modified LP-300 starts weight loss at about 100°C. The thermal weight loss process is complex, as can be seen from the TG and DTG curves, which can be divided into many stages. KOH-modified LP-300 shows significant weight loss at about 750°C–800°C, which is probably due to the volatilization of potassium [29].

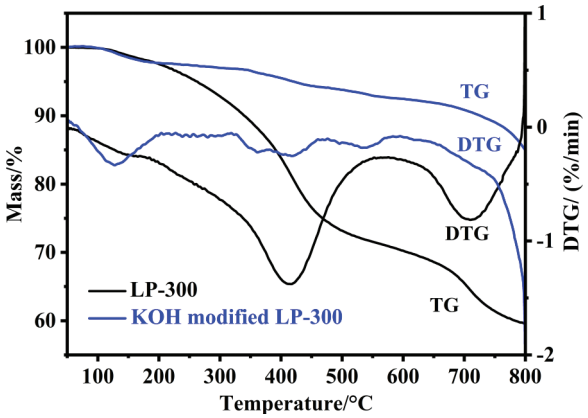

Figure 5: TG/DTG curves of LP-300 and the KOH-modified LP-300 for preparation of PC-3 in Ar atmosphere

To elucidate the reaction mechanism of KOH activation, mass spectrometry (MS) was employed to detect the gases released during TG analysis. Four gaseous products with mass-to-charge (m/z) ratios of 2, 18, 28 and 44 were detected and assigned to H_2, H_2O, CO and CO_2, respectively.

As shown in Fig. 6a, LP-300 initiates hydrogen release at about 369°C, while the KOH-modified LP-300 starts to release hydrogen at around 317°C. KOH has significantly promoted the low-temperature dehydrogenation reaction, which is mainly due to the reaction of KOH with carbon (Eq. (1)) [30–32]. When the temperature exceeds 500°C, the hydrogen released by LP-300 gradually decreases, while the hydrogen released by the KOH-modified LP-300 remains stable and even increases after 750°C. The high-temperature dehydrogenation reaction may be attributed to the removal of hydrogen atoms at the edge of lignin-derived amorphous carbon [33]. This process is essential for the transformation of disordered amorphous carbon into ordered graphite-like carbon. Fig. 6b displays the MS curve of H_2O with an m/z of 18 for LP-300 and KOH-modified LP-300. It is evident that the KOH-modified LP-300 shows a peak at about 369°C, which occurs earlier than that of the unmodified LP-300. This suggests that the addition of KOH may promote the dehydration of lignin molecules. In addition, KOH undergoes thermal decomposition at about 400°C, resulting in the formation of H_2O and K_2O (Eq. (2)) [26]. Fig. 6c depicts the MS curve of CO for LP-300 and KOH-modified LP-300. There is a significant difference in these MS curves above 700°C. The release of CO from LP-300 begins to decrease significantly, and tends to stabilize at 800°C, suggesting that the carbonization process of LP-300 concludes at this temperature. In contrast, the release of CO from KOH-modified LP-300 continues to increase after 700°C, which is attributed to the reaction of K_2O and carbon (Eq. (6)) [34]. The MS curve of CO_2 for

LP-300 and KOH-modified LP-300 is shown in Fig. 6d. LP-300 begins to release CO_2 at about 130°C, which may be attributed to the decarboxylation reaction and the desorption of CO_2 absorbed in lignin. In contrast, KOH-modified LP-300 does not exhibit a CO_2 signal before 330°C, which is probably due to the reaction between CO_2 and KOH (Eq. (3)). The released CO_2 was absorbed and reacted by KOH. KOH-modified LP-300 displays two new CO_2 peaks at 550°C and 790°C, which may be caused by the decomposition of $KHCO_3$ and K_2CO_3, respectively (Eqs. (4) and (5)).

$$4KOH + C \rightarrow K_2CO_3 + K_2O + 2H_2 \quad (1)$$

$$2KOH \rightarrow K_2O + H_2O \quad (2)$$

$$KOH + CO_2 \rightarrow KHCO_3 \quad (3)$$

$$2KHCO_3 \rightarrow K_2CO_3 + H_2O + CO_2 \quad (4)$$

$$K_2CO_3 \rightarrow K_2O + CO_2 \quad (5)$$

$$K_2O + 2C \rightarrow 2K + CO \quad (6)$$

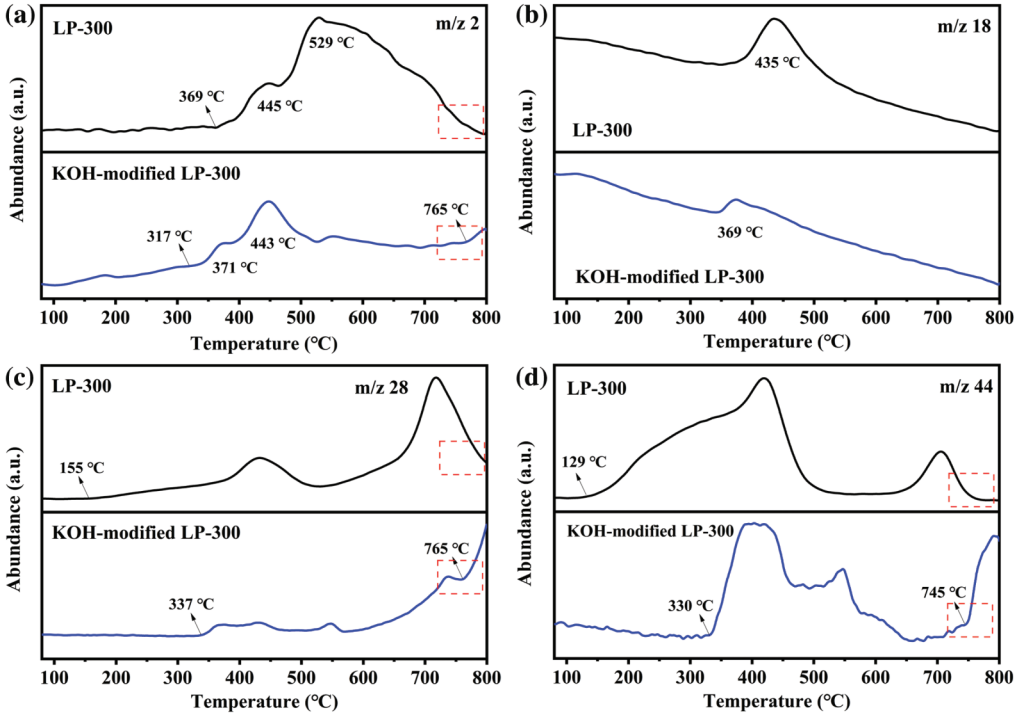

Figure 6: MS curves of released gases (a) H_2, (b) H_2O, (c) CO, (d) CO_2

As can be seen from the above TG-MS results, KOH significantly promotes the removal of H_2 and CO from lignin-derived carbon at high temperatures. The release of a substantial quantity of gaseous molecules not only generates numerous micropores, but also facilitates the formation of ordered carbon structures. The dehydrogenation reaction enables the conversion of more sp^3 hybridized carbon into sp^2 hybridized carbon. CO is a product of the reaction between K_2O and amorphous carbon. An increase in CO indicates that more amorphous carbon is etched and consumed, which in turn preserves more ordered carbon structures.

3.3 Electrochemical Performance of Porous Carbons

The porous carbon was used as a working electrode for a supercapacitor, and its electrochemical performance was evaluated in a three-electrode system using a 6M KOH electrolyte. In Fig. 7a, the cyclic voltammetry (CV) curves of PC-1, PC-2, and PC-3 at a scanning rate of 50 mV s^{-1} are displayed. The CV curves of the three samples exhibit a quasi-rectangular shape with no obvious redox peak, behaving a typical electric double-layer capacitor (EDLC). Subsequently, the galvanostatic charge-discharge (GCD) curves were recorded to further analyze the capacitive performance of the samples. As depicted in Fig. 7b, all the samples exhibit nearly triangular GCD curves, highlighting substantial electrochemical reversibility. Notably, PC-2 exhibits the longest charge and discharge duration, suggesting the highest specific capacitance among the samples. In Fig. 7c, the specific capacitance of PC-1, PC-2, and PC-3 is depicted at various current densities. At current densities of 0.2, 0.5, 1, 2, 5, 10 and 20 A g^{-1}, PC-2 shows specific capacitance values of 256, 214, 199, 188.2, 177, 167 and 160 F g^{-1}, respectively, while PC-3 exhibits values of 172, 139, 130, 123, 114.5, 106 and 96 F g^{-1}, respectively. Both of them are significantly higher than that of PC-1. Even at a current density of 20 A g^{-1}, the specific capacitance of PC-2 and PC-3 retains 60.6% and 55.8%, respectively, relative to the values at 0.2 A g^{-1}. It indicates that the two samples have good rate performance.The excellent capacitance performance of PC-2 in the three-electrode system is mainly attributed to its exceptional pore structure. The synergistic effect of micropores and mesoporous pores makes it an excellent electrode material for supercapacitors.

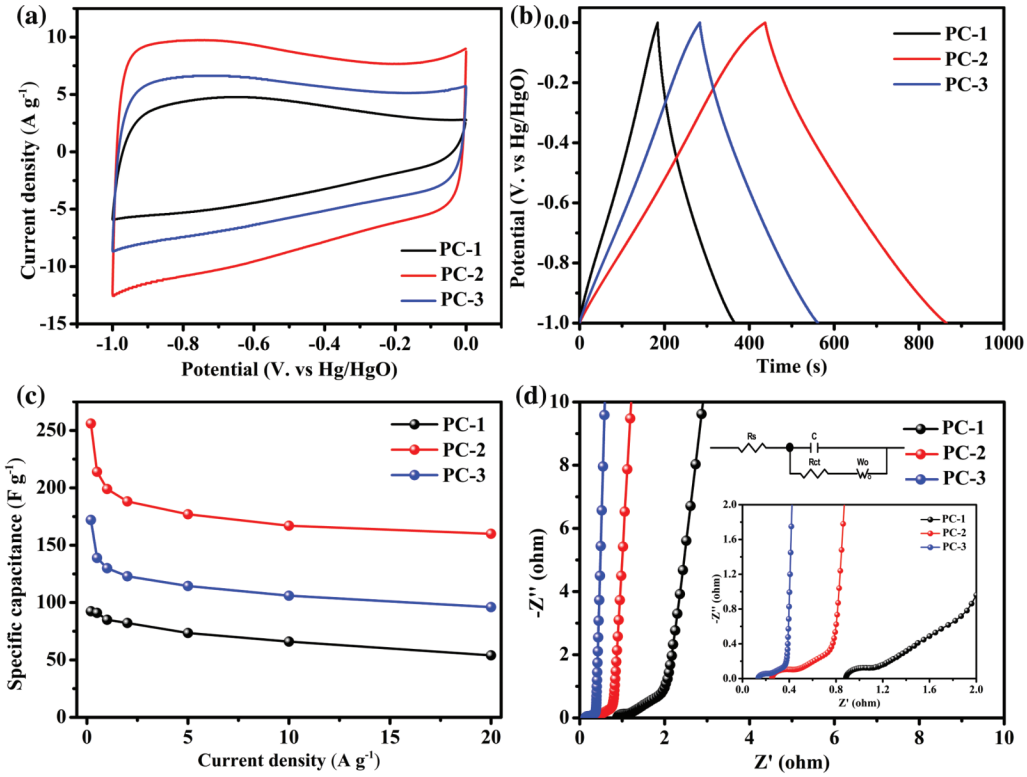

Figure 7: Electrochemical performance of the PC-1, PC-2 and PC-3 electrodes assessed in a three-electrode system using a 6 M KOH aqueous electrolyte. (a) CV curves at a scan rate of 50 mV s^{-1}; (b) GCD curves at a current density of 0.5 A g^{-1}; (c) Specific capacitance at varying current densities; (d) Nyquist plot

Electrochemical impedance spectroscopy (EIS) was employed to further investigate the electrochemical properties of the porous carbons [35]. The Nyquist diagram and equivalent circuit diagram are shown in Fig. 7d. The experimental data from EIS were fitted using ZView software, and the results are presented in Table 2. As shown in the figure, the R_s values of PC-1, PC-2 and PC-3 are 0.89, 0.25 and 0.14 Ω respectively, indicating that the PC-3 sample has the best electrical conductivity in the system. Compared to PC-1, the Nyquist curves of PC-2 and PC-3 are nearly vertical in the low frequency region, indicating a faster charge transfer rate. The 45° diagonal line in the enlarged image is described as the Warburg impedance, which reflects the magnitude of the ion diffusion resistance. The relatively low Wo1-R value of PC-3 indicates its good ion diffusion ability. In the mid to high frequency region of the EIS, the charge transfer resistance (R_{ct}) magnitude is observed. PC-3 displays a small R_{ct}, indicating a minor interfacial migration resistance. The low resistance and high ionic mobility of PC-3 are attributed to its more ordered structure.

Table 2: The impedance data of PC-1, PC-2 and PC-3

Sample	R_s (Ω)	R_{ct} (Ω)	Wo1-R (Ω)
PC-1	0.89	0.191	2.85
PC-2	0.25	0.169	1.12
PC-3	0.14	0.085	0.50

Note: R_s: solution resistance. R_{ct}: charge transfer resistance. Wo1-R: diffusion resistance of electrolyte ions.

4 Conclusion

In this work, lignin was converted into porous carbons by spray drying and KOH activation. The thermochemical conversion process was investigated using thermogravimetric mass spectrometry (TG-MS). With the increase of the KOH ratio, the specific surface area and structural order of the resulting porous carbon continued to increase. At a sample-to-KOH ratio of 1:3, the resulting porous carbon (PC-3) exhibited a specific surface area of 2400 m^2/g and a distinct graphite-like ordered structure. TG-MS confirmed that KOH facilitated the removal of hydrogen and CO. The dehydrogenation reaction made more sp^3 hybridized carbon be converted into sp^2 hybridized carbon. The released CO was derived from the reaction between K_2O and amorphous carbon. As more CO was removed, a greater amount of amorphous carbon was consumed, and a more ordered carbon structure was left. PC-3 exhibited a higher specific surface area, more ordered structure, and lower resistance. However, its capacitance performance was not optimal. The porous carbon (PC-2) possessed a larger quantity of both micropores and mesopores, resulting in a higher capacitance of 256 F g^{-1} at a current density of 0.2 A g^{-1}. The pore structure had a more pronounced impact on the electrochemical performance of the porous carbon compared to the carbon structure. This study offered valuable insights into the preparation of lignin-derived porous carbons for high-performance supercapacitors.

Acknowledgement: None.

Funding Statement: The research received funding from the Key Research and Development Projects of Zhejiang Province (2022C01236) and the Ningbo Top Talent Project.

Author Contributions: Conceptualization; Data Curation; Formal Analysis; Visualization; Roles/Writing-Original Draft: Shihao Feng. Conceptualization, Formal Analysis; Writing-Review & Editing, Supervision, Visualization: Qin Ouyang. Validation; Visualization; Data Curation: Jing Huang. Validation; Supervision; Resources; Software: Xilin Zhang. Validation; Supervision; Resources: Ma Zongjun. Resources, Supervision: Kun Liang. Supervision; Project Administration; Resources: Qing Huang. All authors reviewed the results and approved the final version of the manuscript.

Availability of Data and Materials: Data available on request from the authors.

Conflicts of Interest: The authors declare that they have no conflicts of interest to report regarding the present study.

References

1. Cai J, He Y, Yu X, Banks SW, Yang Y, Zhang X, et al. Review of physicochemical properties and analytical characterization of lignocellulosic biomass. Renew Sust Energ Rev. 2017;76:309–22. doi:10.1016/j.rser.2017.03.072.
2. Tan X, Tan T. Biofuels from biomass toward a net-zero carbon and sustainable world. Joule. 2022;6(7):1396–9. doi:10.1016/j.joule.2022.06.005.
3. Lobato-Peralta DR, Duque-Brito E, Villafán-Vidales HI, Longoria A, Sebastian PJ, Cuentas-Gallegos AK, et al. A review on trends in lignin extraction and valorization of lignocellulosic biomass for energy applications. J Clean Prod. 2021;293:126123. doi:10.1016/j.jclepro.2021.126123.
4. Chen Z, Chen L, Khoo KS, Gupta VK, Sharma M, Show PL, et al. Exploitation of lignocellulosic-based biomass biorefinery: a critical review of renewable bioresource, sustainability and economic views. Biotechnol Adv. 2023;69:108265. doi:10.1016/j.biotechadv.2023.108265.
5. Cao KLA, Kitamoto Y, Iskandar F, Ogi T. Sustainable porous hollow carbon spheres with high specific surface area derived from Kraft lignin. Adv Powder Technol. 2021;32(6):2064–73. doi:10.1016/j.apt.2021.04.012.
6. Kitamoto Y, Cao KLA, Le PH, Abdillah OB, Iskandar F, Ogi T. A sustainable approach for preparing porous carbon spheres derived from kraft lignin and sodium hydroxide as highly packed thin film electrode materials. Langmuir. 2022;38(11):3540–52. doi:10.1021/acs.langmuir.1c03489.
7. Liu D, Ouyang Q, Jiang X, Ma H, Chen Y, He L. Thermal properties and thermal stabilization of lignosulfonate-acrylonitrile-itaconic acid terpolymer for preparation of carbon fiber. Polym Degrad Stab. 2018;150(6185):57–66. doi:10.1016/j.polymdegradstab.2018.02.013.
8. Song L, Ouyang Q, Huang X, Ma H, Chen P, Shen L, et al. Carbon fibers with low cost and uniform disordered structure derived from lignin/polyacrylonitrile composite precursors. Fiber Polym. 2021;22(1):240–8. doi:10.1007/s12221-021-9414-5.
9. Zhou X, Jin C, Liu G, Wu G, Huo S, Kong Z. Functionalized lignin-based magnetic adsorbents with tunable structure for the efficient and selective removal of Pb(II) from aqueous solution. Chem Eng J. 2021;420(420):130409. doi:10.1016/j.cej.2021.130409.
10. Shi F, Li J, Xiao J, Zhao X, Li H, An Q, et al. Three-dimensional hierarchical porous lignin-derived carbon/WO3 for high-performance solid-state planar micro-supercapacitor. Int J Biol Macromol. 2021;190:11–8. doi:10.1016/j.ijbiomac.2021.08.183.
11. Shi F, Zhao S, Yang J, Tong Y, Li J, Zhai S, et al. Nickel-cobalt bimetallic tungstate decorated 3D hierarchical porous carbon derived from lignin for high-performance supercapacitor applications. J Mater Chem A. 2022;10(23):12679–91. doi:10.1039/D2TA01636B.
12. Tong Y, Yang J, Li J, Cong Z, Li W, Liu M, et al. Lignin-derived electrode materials for supercapacitor applications: progress and perspective. J Mater Chem A. 2023;11(3):061–1082.
13. Xia K, Ouyang Q, Chen Y, Wang X, Qian X, Wang L. Preparation and characterization of lignosulfonate-acrylonitrile copolymer as a novel carbon fiber precursor. ACS Sustain Chem Eng. 2015;4(1):159–68.
14. Shi F, Tong Y, Li H, Li J, Cong Z, Zhai S, et al. Synthesis of oxygen/nitrogen/sulfur codoped hierarchical porous carbon from enzymatically hydrolyzed lignin for high-performance supercapacitors. J Energy Storage. 2022;52:104992. doi:10.1016/j.est.2022.104992.
15. Li H, Shi F, An Q, Zhai S, Wang K, Tong Y. Three-dimensional hierarchical porous carbon derived from lignin for supercapacitors: insight into the hydrothermal carbonization and activation. Int J Biol Macromol. 2021;166:923–33. doi:10.1016/j.ijbiomac.2020.10.249.

16. Qin Q, Zhong F, Song T, Yang Z, Zhang P, Cao H, et al. Optimization of multiscale structure and electrochemical properties of bamboo-based porous activated biochar by coordinated regulation of activation and air oxidation. Chem Eng J. 2023;477(8):146763. doi:10.1016/j.cej.2023.146763.
17. Qin Z, Ye Y, Zhang D, He J, Zhou J, Cai J. One/two-step contribution to prepare hierarchical porous carbon derived from rice husk for supercapacitor electrode materials. ACS Omega. 2023;8(5):5088–96. doi:10.1021/acsomega.2c07932.
18. Yue X, Yang H, Cao Y, Jiang L, Li H, Shi F, et al. Nitrogen-doped cornstalk-based biomass porous carbon with uniform hierarchical pores for high-performance symmetric supercapacitors. J Mat Sci. 2022;57(5):3645–61. doi:10.1007/s10853-022-06891-9.
19. Lu CY, Wey MY, Chuang KH. Catalytic treating of gas pollutants over cobalt catalyst supported on porous carbons derived from rice husk and carbon nanotube. Appl Catal B: Environ. 2009;90(3–4):652–61. doi:10.1016/j.apcatb.2009.04.030.
20. Zhang J, Zhang C, Zhao Y, Amiinu IS, Zhou H, Liu X, et al. Three dimensional few-layer porous carbon nanosheets towards oxygen reduction. Appl Catal B: Environ. 2017;211:148–56. doi:10.1016/j.apcatb.2017.04.038.
21. Li B, Li J, Guo M. Preparation of low internal resistance electrode material with multistage interconnected pores from coffee grounds. Adv Compos Hybrid Mater. 2024;7(2):48. doi:10.1007/s42114-024-00858-x.
22. Shan L, Zhang Y, Xu Y, Gao M, Xu T, Si C. Wood-based hierarchical porous nitrogen-doped carbon/manganese dioxide composite electrode materials for high-rate supercapacitor. Adv Compos Hybrid Mater. 2023;6(5):174. doi:10.1007/s42114-023-00744-y.
23. Tan Z, Yang J, Liang Y, Zheng M, Hu H, Dong H, et al. The changing structure by component: biomass-based porous carbon for high-performance supercapacitors. J Colloid Interface Sci. 2021;585:778–86. doi:10.1016/j.jcis.2020.10.058.
24. Wang T, Liu Z, Li P, Wei H, Wei K, Chen X. Lignin-derived carbon aerogels with high surface area for supercapacitor applications. Chem Eng J. 2023;466:143118. doi:10.1016/j.cej.2023.143118.
25. Wang K, Xu M, Gu Y, Gu Z, Fan QH. Symmetric supercapacitors using urea-modified lignin derived N-doped porous carbon as electrode materials in liquid and solid electrolytes. J Power Sources. 2016;332:180–6. doi:10.1016/j.jpowsour.2016.09.115.
26. Otowa T, Tanibata R, Itoh M. Production and adsorption characteristics of MAXSORB: high-surface-area active carbon. Gas Sep & Purif. 1993;7(4):241–5. doi:10.1016/0950-4214(93)80024-Q.
27. Feng S, Fan Q, Ouyang Q, Zhang X, Liang K, Huang Q. Morphology and structure control of lignin-derived hierarchical porous carbon for high-performance supercapacitors. Colloid Surface A. 2024;685:133292. doi:10.1016/j.colsurfa.2024.133292.
28. Niu Q, Gao K, Tang Q, Wang L, Han L, Fang H, et al. Large-size graphene-like porous carbon nanosheets with controllable N-doped surface derived from sugarcane bagasse pith/chitosan for high performance supercapacitors. Carbon. 2017;123:290–8. doi:10.1016/j.carbon.2017.07.078.
29. Wang X, Chen Q, Wei B, Yu G, Li H, Chen X, et al. Volatile potassium transfer behavior in carbon matrix and its effect on char gasification. Fuel. 2023;333:126302. doi:10.1016/j.fuel.2022.126302.
30. Lozano-Castelló D, Calo JM, Cazorla-Amorós D, Linares-Solano A. Carbon activation with KOH as explored by temperature programmed techniques, and the effects of hydrogen. Carbon. 2007;45(13):2529–36. doi:10.1016/j.carbon.2007.08.021.
31. Raymundo-Piñero E, Azaïs P, Cacciaguerra T, Cazorla-Amorós D, Linares-Solano A, Béguin F. KOH and NaOH activation mechanisms of multiwalled carbon nanotubes with different structural organisation. Carbon. 2005;43(4):786–5. doi:10.1016/j.carbon.2004.11.005.
32. Qiao WM, Yoon SH, Mochida I. KOH activation of needle coke to develop activated carbons forHigh-performance EDLC. Energ Fuel. 2006;20(4):1680–4. doi:10.1021/ef050313l.
33. Wang B, Hu J, Chen W, Chang C, Pang S, Li P. Exploring the characteristics of coke formation on biochar-based catalysts during the biomass pyrolysis. Fuel. 2024;357(10):129859. doi:10.1016/j.fuel.2023.129859.

34. Wang H, Gao Q, Hu J. High hydrogen storage capacity of porous carbons preparedby using activated carbon. J Am Chem Soc. 2009;131(20):7016–22. doi:10.1021/ja8083225.
35. Zhang X, Feng S, Yu J, Shi R, Ma Z, Yang Z, et al. Tuning d orbital of Ni single atom by encapsulating ni nanoparticle in carbon nanotube for efficient oxygen evolution reaction. Energ Fuel. 2022;36(21):13159–67. doi:10.1021/acs.energyfuels.2c02644.